

A Calculation of Rotor Impedance for Hovering Articulated-Rotor Helicopters

Kanichiro Kato* and Takashi Yamane†
University of Tokyo, Tokyo, Japan

A procedure is presented to calculate the loads transferred from an articulated rotor to the fuselage when the rotor hub is forced to oscillate sinusoidally in hover. The blade is considered as a rotating elastic beam and the inertial load expressions are given for the case where the hub is in motion. Basis assumptions include: 1) quasisteady aerodynamic loads, 2) integration with strip theory, and 3) neglect of the effects of preceding and returning wakes. Sample calculations reveal the manner in which the typical articulated rotor impedances are influenced by blade elastic deformations, inertial loads, aerodynamic loads, and hub frequencies.

I. Introduction

IN rotary wing aeroelastic problems, as the recent review by Friedmann¹ shows, coupled rotor-fuselage problems have been implemented by somewhat sophisticated computer programs. Typical programs²⁻⁴ consist of a dynamic and aerodynamic description of fully coupled main or tail rotor/airframe/control systems and give time history solution, vibration level, motion eigenvalues and mode shapes, airloadings, stresses, trim, and so forth.

In these mathematical simulations, rotorcrafts are usually broken down into major subsystems such as rotor blades, airframe system, and control systems; and each of these is treated separately. Total dynamic responses are composed through the motions of the respective coupling generalized coordinates. Blade aerodynamics are ordinarily treated in the following manner. Airloads are integrated by strip theory and the local airloads are obtained either by table lookup of the blade section properties or by the two-dimensional unsteady thin-airfoil theory, or by the proper combination of the two methods. In the table lookup, dynamic stall can be approximately taken care of, while in unsteady aerodynamics, the lift deficiency function typically can have three expressions: Theodorsen function, Loewy's function, and unity. The last one corresponds to so-called quasisteady aerodynamics.

When using these programs, important insight will be obtained if one knows the frequency responses of the rotors against hub motions. It will also serve for rotor design optimizations. In view of this, this paper formulates the procedure to calculate the rotor impedances for flexible blades and gives sample calculations for a hovering articulated rotor. Two-dimensional quasisteady aerodynamic strip theory is used for blade airload calculations. This means that the airloads are taken higher than the exact ones and the effects of preceding or returning wakes are neglected.

If the air density is set equal to zero, this calculation gives the rotor impedances due to inertial loads only. Sample calculations include the comparisons of the cases with and without the airloads, which define the two extreme bounds of rotor impedances. These calculations will disclose the essential features of the rotor impedances as well as the frequency ranges where aerodynamic effects may be significant.

II. Coordinate Systems and Motion Variables

The following five right-handed orthogonal frames are used to describe the blade and the hub motions.

1) Inertial Frame (I-frame) $X_I Y_I Z_I$ - This frame coincides with the S-frame under the steady-state flight condition.

2) Shaft Frame (S-frame) $X_S Y_S Z_S$ - This frame is fixed to the fuselage with its origin at the hub center. Z_S coincides with the rotor shaft and X_S is taken in the plane of symmetry (Fig. 1). This frame is related to the I-frame by the following transformation using Euler angles (ϕ_x, ϕ_y, ϕ_z) , as shown in Fig. 2:

$$\begin{Bmatrix} X_I \\ Y_I \\ Z_I \end{Bmatrix} = [\Phi] \begin{Bmatrix} X_S \\ Y_S \\ Z_S \end{Bmatrix} + \begin{Bmatrix} x_h \\ y_h \\ z_h \end{Bmatrix} \quad (1)$$

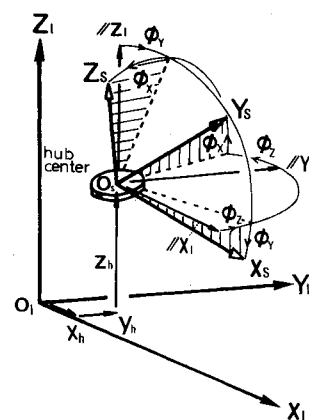


Fig. 1 Hub motion degrees of freedom.

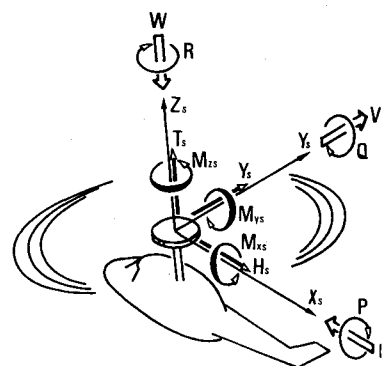


Fig. 2 Hub motions and hub loads.

Received May 6, 1977; revision received Aug. 1, 1978. Copyright © 1978 by Kanichiro Kato and Takashi Yamane, with release to AIAA to publish in all forms.

Index categories: Helicopters; Vibration; Aeroelasticity and Hydroelasticity.

*Associate Professor, Department of Aeronautics.

†Graduate Student, Department of Aeronautics.

where

$$[\Phi] = \begin{bmatrix} \cos\phi_z - \sin\phi_z & 0 \\ \sin\phi_z & \cos\phi_z & 0 \\ 0 & 0 & 1 \end{bmatrix} \begin{bmatrix} \cos\phi_y & 0 & \sin\phi_y \\ 0 & 1 & 0 \\ -\sin\phi_y & 0 & \cos\phi_y \end{bmatrix} \\ \times \begin{bmatrix} 1 & 0 & 0 \\ 0 & \cos\phi_x & -\sin\phi_x \\ 0 & \sin\phi_x & \cos\phi_x \end{bmatrix}$$

The velocity and angular velocity of the hub are denoted as $(-U, V, -W)$ and $(-P, Q, -R)$, respectively, in the S-frame according to the sign convention of the airplane dynamics (refer to Fig. 1). They are related to $(\dot{x}_h, \dot{y}_h, \dot{z}_h)$ and $(\dot{\phi}_x, \dot{\phi}_y, \dot{\phi}_z)$ as follows:

$$\begin{Bmatrix} -U \\ V \\ -W \end{Bmatrix} = [\Phi]^T \begin{Bmatrix} \dot{x}_h \\ \dot{y}_h \\ \dot{z}_h \end{Bmatrix} \quad (2)$$

$$\begin{Bmatrix} -P \\ Q \\ -R \end{Bmatrix} = \begin{bmatrix} 1 & 0 & -\sin\phi_y \\ 0 & \cos\phi_x & \sin\phi_x \cos\phi_y \\ 0 & -\sin\phi_x & \cos\phi_x \cos\phi_y \end{bmatrix} \begin{Bmatrix} \dot{\phi}_x \\ \dot{\phi}_y \\ \dot{\phi}_z \end{Bmatrix} \quad (3)$$

For small shaft inclinations ($|\phi_x|, |\phi_y|, |\phi_z| \ll 1$), they are approximated as

$$\begin{Bmatrix} -U \\ V \\ -W \end{Bmatrix} \equiv \begin{Bmatrix} \dot{x}_h \\ \dot{y}_h \\ \dot{z}_h \end{Bmatrix} \quad \begin{Bmatrix} -P \\ Q \\ -R \end{Bmatrix} \equiv \begin{Bmatrix} \dot{\phi}_x \\ \dot{\phi}_y \\ \dot{\phi}_z \end{Bmatrix} \quad (4)$$

3) Rotating Hub Frame (R-frame) $X_R Y_R Z_R$ —This frame is the one when the S-frame is rotated about Z_S by $\psi = \Omega t$, as is shown in Fig. 3. Ω is the shaft rotational speed which will be assumed constant. Coordinate transformation between an S- and R-frame is

$$\begin{Bmatrix} X_S \\ Y_S \\ Z_S \end{Bmatrix} = [\Psi] \begin{Bmatrix} X_R \\ Y_R \\ Z_R \end{Bmatrix}$$

where

$$[\Psi] = \begin{bmatrix} \cos\psi & -\sin\psi & 0 \\ \sin\psi & \cos\psi & 0 \\ 0 & 0 & 1 \end{bmatrix} \quad (5)$$

In this paper, the undeformed blade elastic axis is assumed to be a straight line which coincides with the feathering axis and the area centroid. Referring to Fig. 3, the undeformed elastic axis is located at $Y_R = e_0, Z_R = 0$. This rotating frame

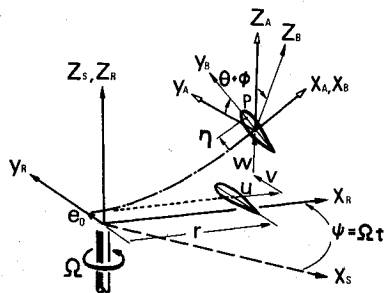


Fig. 3 Blade deformations.

will be used to describe the blade deformations and load distributions.

4) Blade Frame (B-frame) $X_B Y_B Z_B$ —This is a local frame fixed to each blade section considered. The blade section itself is assumed to be rigid. X_B is directed outward along the local elastic axis, while Y_B is directed toward the zero-lift angle of the blade section. The displacements of the elastic axis is denoted by (u, v, w) in the R-frame. Angular position relative to the R-frame is given by the three Euler angles $(\theta + \phi, -w', v')$, where $()'$ denotes $\partial() / \partial X_R$. v' and $-w'$ are lead and flap angle, respectively, while θ and ϕ denote pitch setting angle and elastic torsional deformation, respectively. The coordinate transformation between an R- and B-frame is

$$\begin{Bmatrix} X_R \\ Y_R \\ Z_R \end{Bmatrix} = [\Delta] \begin{Bmatrix} X_B \\ Y_B \\ Z_B \end{Bmatrix} + \begin{Bmatrix} r+u \\ e_0+v \\ w \end{Bmatrix} \quad (6)$$

where

$$[\Delta] = \begin{bmatrix} 1 & -v' & 0 \\ v' & 1 & 0 \\ 0 & 0 & 1 \end{bmatrix} \begin{bmatrix} 1 & 0 & -w' \\ 0 & 1 & 0 \\ w' & 0 & 1 \end{bmatrix} \\ \times \begin{bmatrix} 1 & 0 & 0 \\ 0 & \cos(\theta + \phi) & -\sin(\theta + \phi) \\ 0 & \sin(\theta + \phi) & \cos(\theta + \phi) \end{bmatrix} \\ \equiv \begin{bmatrix} 1 & -v' - \theta w' & -w' + \theta v' \\ v' & 1 - \theta^2/2 - \theta\phi & -\theta - \phi \\ w' & \theta + \phi & 1 - \theta^2/2 - \theta\phi \end{bmatrix}$$

5) Aerodynamic Frame (A-frame) $X_A Y_A Z_A$ —This is also a local frame which is obtained by setting $\theta + \phi \equiv 0$ in the B-frame, that is, Y_A stays parallel to the $X_R Y_R$ plane. The coordinate transformation between an R- and A-frame is

$$\begin{Bmatrix} X_R \\ Y_R \\ Z_R \end{Bmatrix} = [\Delta_A] \begin{Bmatrix} X_A \\ Y_A \\ Z_A \end{Bmatrix} + \begin{Bmatrix} r+u \\ e_0+v \\ w \end{Bmatrix} \quad (7)$$

where

$$[\Delta_A] = \begin{bmatrix} 1 & -v' & 0 \\ v' & 1 & 0 \\ 0 & 0 & 1 \end{bmatrix} \begin{bmatrix} 1 & 0 & -w' \\ 0 & 1 & 0 \\ w' & 0 & 1 \end{bmatrix} \\ \equiv \begin{bmatrix} 1 & -v' - w' \\ v' & 1 & 0 \\ w' & 0 & 1 \end{bmatrix}$$

III. Inertial Loads

Referring to Fig. 3, a point P is considered on the blade whose coordinate is $(0, \eta, 0)$ in the B-frame, which will be expressed in the R-frame as

$$\bar{\xi} = \{\xi\} = [\Delta] \begin{Bmatrix} 0 \\ \eta \\ 0 \end{Bmatrix} + \begin{Bmatrix} r+u \\ e_0+v \\ w \end{Bmatrix} \quad (8)$$

The position vector of P from O_I is given by $\vec{x}_0 + \vec{\xi}$, where \vec{x}_0 denotes $\vec{O}_I\vec{O}_R$ or (x_h, y_h, z_h) in the I-frame. The velocity and the acceleration of P can be obtained by

$$\begin{aligned} \frac{d}{dt}(\vec{x}_0 + \vec{\xi}) &= \frac{d\vec{x}_0}{dt} + \frac{d_*\vec{\xi}}{dt} + \vec{\omega} \times \vec{\xi} \frac{d^2}{dt^2}(\vec{x}_0 + \vec{\xi}) \\ &= \frac{d^2\vec{x}_0}{dt^2} + \frac{d_*^2\vec{\xi}}{dt^2} + 2\vec{\omega} \times \frac{d_*\vec{\xi}}{dt} + \vec{\omega} \times (\vec{\omega} \times \vec{\xi}) + \frac{d_*\vec{\omega}}{dt} \times \vec{\xi} \quad (9) \end{aligned}$$

where $d_*()/dt$ denotes the rate of change as viewed in the R-frame, and $\vec{\omega}$ and $d_*\vec{\omega}/dt$ can be given in the R-frame by

$$\vec{\omega} = \begin{Bmatrix} \Omega_1 \\ \Omega_2 \\ \Omega_3 + \Omega \end{Bmatrix} \quad \frac{d_*\vec{\omega}}{dt} = \begin{Bmatrix} \dot{\Omega}_1 + \Omega\Omega_2 \\ \dot{\Omega}_2 - \Omega\Omega_1 \\ \dot{\Omega}_3 \end{Bmatrix} \quad (10)$$

where

$$\begin{aligned} \begin{Bmatrix} \Omega_1 \\ \Omega_2 \\ \Omega_3 \end{Bmatrix} &\equiv \begin{Bmatrix} -P\cos\psi + Q\sin\psi \\ P\sin\psi + Q\cos\psi \\ -R \end{Bmatrix} \begin{Bmatrix} \dot{\Omega}_1 \\ \dot{\Omega}_2 \\ \dot{\Omega}_3 \end{Bmatrix} \\ &\equiv \begin{Bmatrix} -\dot{P}\cos\psi + \dot{Q}\sin\psi \\ \dot{P}\sin\psi + \dot{Q}\cos\psi \\ -\dot{R} \end{Bmatrix} \quad (11) \end{aligned}$$

and

$$\begin{aligned} \frac{d\vec{x}_0}{dt} &= \begin{Bmatrix} V_1 \\ V_2 \\ V_3 \end{Bmatrix} \equiv \begin{Bmatrix} -U\cos\psi + V\sin\psi \\ U\sin\psi + V\cos\psi \\ -W \end{Bmatrix} \\ \frac{d^2\vec{x}_0}{dt^2} &= \begin{Bmatrix} \dot{V}_1 \\ \dot{V}_2 \\ \dot{V}_3 \end{Bmatrix} \equiv [\Psi]^T \begin{Bmatrix} -(\dot{U} + QW - RV) \\ \dot{V} + RU - PW \\ -(\dot{W} + PV - QU) \end{Bmatrix} \quad (12) \end{aligned}$$

Expanding Eq. (9), the velocity $\{u_R\}$ and the acceleration $\{a_R\}$ of P are reduced to the following, where $\{\dot{\xi}\}$ denotes $d_*\vec{\xi}/dt$:

$$\{u_R\} = \begin{Bmatrix} V_1 \\ V_2 \\ V_3 \end{Bmatrix} + \{\dot{\xi}\} + \begin{Bmatrix} \Omega_1 \\ \Omega_2 \\ \Omega_3 + \Omega \end{Bmatrix} \times \{\xi\} \quad (13)$$

$$\begin{aligned} \{a_R\} &= \begin{Bmatrix} \dot{V}_1 \\ \dot{V}_2 \\ \dot{V}_3 \end{Bmatrix} + \{\ddot{\xi}\} + 2 \begin{Bmatrix} \Omega_1 \\ \Omega_2 \\ \Omega_3 + \Omega \end{Bmatrix} \times \{\dot{\xi}\} \\ &+ \begin{Bmatrix} \Omega_1 \\ \Omega_2 \\ \Omega_3 + \Omega \end{Bmatrix} \times \left(\begin{Bmatrix} \Omega_1 \\ \Omega_2 \\ \Omega_3 + \Omega \end{Bmatrix} \times \{\xi\} \right) + \begin{Bmatrix} \dot{\Omega}_1 + \Omega\Omega_2 \\ \dot{\Omega}_2 - \Omega\Omega_1 \\ \dot{\Omega}_3 \end{Bmatrix} \times \{\xi\} \quad (14) \end{aligned}$$

Chordwise integration of inertial loads given by

$$\{\bar{P}\} = - \int_{\text{chord}} \{a_R\} dm \quad \{\bar{Q}\} = - \int_{\text{chord}} \{\eta_R\} \times \{a_R\} dm \quad (15)$$

where

$$\{\eta_R\} = [\Delta] \begin{Bmatrix} 0 \\ \eta \\ 0 \end{Bmatrix} \cong \eta \begin{Bmatrix} -v' - \theta w' \\ 1 - \theta^2/2 - \theta\phi \\ \theta + \phi \end{Bmatrix}$$

results in the inertial forces $\{\bar{P}\}$ and moments $\{\bar{Q}\}$ acting on unit span, where dm is the chordwise mass density per unit span. Laborious, straightforward calculation will give the following results:

$$\{\bar{P}\} \equiv \begin{Bmatrix} f_x \\ f_y \\ f_z \end{Bmatrix} + \begin{Bmatrix} \bar{p}_x \\ \bar{p}_y \\ \bar{p}_z \end{Bmatrix} \quad (16)$$

$$\begin{aligned} \begin{Bmatrix} f_x \\ f_y \\ f_z \end{Bmatrix} &= \\ -m \begin{Bmatrix} \dot{V}_1 + (e\theta + w_0)\dot{\Omega}_2 - (e_0 + e)\dot{\Omega}_3 - 2r\Omega\Omega_3 \\ \dot{V}_2 - (e\theta + w_0)\dot{\Omega}_1 + r\dot{\Omega}_3 - 2(e_0 + e)\Omega\Omega_3 \\ \dot{V}_3 + (e_0 + e)\dot{\Omega}_1 - r\dot{\Omega}_2 + 2r\Omega\Omega_1 + 2(e_0 + e)\Omega\Omega_2 \end{Bmatrix} & \quad (16a) \end{aligned}$$

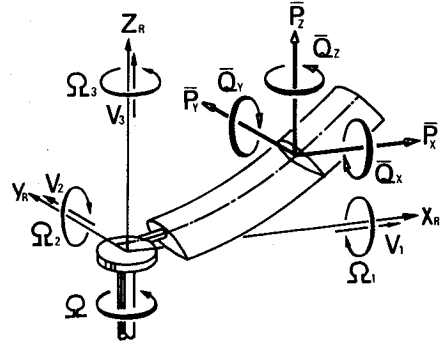


Fig. 4 Blade section loads.

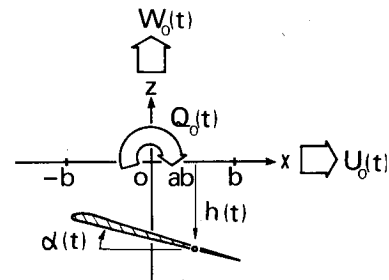


Fig. 5a Two-dimensional thin airfoil theory.

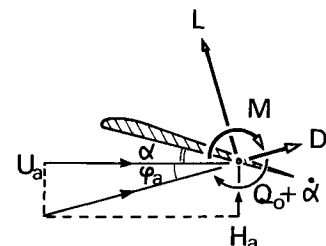


Fig. 5b Directions of lift and drag.

$$\begin{Bmatrix} \bar{p}_x \\ \bar{p}_y \\ \bar{p}_z \end{Bmatrix} = -m \begin{Bmatrix} \ddot{u} - e(\ddot{v}' + \theta\ddot{w}') + 2\Omega[-\dot{v} + e\theta(\dot{\theta} + \dot{\phi})] - \Omega^2[r + u - e(v' + \theta w')] \\ \ddot{v} - e\theta(\ddot{\theta} + \ddot{\phi}) + 2\Omega[\dot{u} - e(\dot{v}' + \theta\dot{w}')] - \Omega^2[e_0 + e + v - e\theta\phi] \\ \ddot{w} + e(\ddot{\theta} + \ddot{\phi}) \end{Bmatrix} \quad (16b)$$

$$\{\bar{Q}\} \equiv \begin{Bmatrix} m_x \\ m_y \\ m_z \end{Bmatrix} + \begin{Bmatrix} \bar{q}_x \\ \bar{q}_y \\ \bar{q}_z \end{Bmatrix} \quad (17)$$

$$\begin{Bmatrix} m_x \\ m_y \\ m_z \end{Bmatrix} = -mk^2 \begin{Bmatrix} \dot{\Omega}_1 + 2\Omega(\Omega_2 + \theta\Omega_3) \\ -\theta\dot{\Omega}_3 \\ -\theta\dot{\Omega}_2 + \dot{\Omega}_3 \end{Bmatrix} - me \begin{Bmatrix} \dot{V}_3 + e_0\dot{\Omega}_1 - r\dot{\Omega}_2 + 2\Omega(r\Omega_1 + e_0\Omega_2) - \theta(\dot{V}_2 - w_0\dot{\Omega}_1 + r\dot{\Omega}_3 - 2e_0\Omega\Omega_3) \\ \theta(\dot{V}_1 + w_0\dot{\Omega}_2 - e_0\dot{\Omega}_3 - 2r\Omega\Omega_3) \\ -(\dot{V}_1 + w_0\dot{\Omega}_2 - e_0\dot{\Omega}_3 - 2r\Omega\Omega_3) \end{Bmatrix} \quad (17a)$$

$$\begin{Bmatrix} \bar{q}_x \\ \bar{q}_y \\ \bar{q}_z \end{Bmatrix} = -mk^2 \begin{Bmatrix} \ddot{\theta} + \ddot{\phi} + \Omega^2(\theta + \phi) + 2\Omega\theta\dot{v}' \\ -\theta\ddot{v}' + \Omega^2\theta v' \\ \ddot{v}' + \theta\ddot{w}' - 2\Omega\theta(\dot{\theta} + \dot{\phi}) \end{Bmatrix} - me \begin{Bmatrix} \ddot{w} - \theta[\ddot{v} + 2\Omega\dot{u} - \Omega^2(e_0 + v)] + e_0\Omega^2\phi \\ \theta[\ddot{u} - 2\Omega\dot{v} - \Omega^2(r + u)] - r\Omega^2\phi \\ -[\ddot{u} - 2\Omega\dot{v} - \Omega^2(r + u)] - r\Omega^2\theta\phi + e_0\Omega^2(v' + \theta w') \end{Bmatrix} \quad (17b)$$

where w_0 denotes the trim value of w , and

$$m = \int_{\text{chord}} dm \quad e = \frac{1}{m} \int_{\text{chord}} \eta dm \quad k = \left(\frac{1}{m} \int_{\text{chord}} \eta^2 dm \right)^{1/2}$$

are mass, distance between mass and elastic axis, and polar radius of gyration of the blade per unit span, respectively. In the preceding derivations, small disturbances have been assumed for U , V , W , P , Q , R , u , v , and ϕ (except for w) and the small-angle assumption ($\sin\theta \approx \theta$ and $\cos\theta \approx 1 - \theta^2/2$) has been made for θ .

Equations (16a) and (17a) are the loads caused by the hub motions and have the same expressions when calculated as if the rotor were a rigid propeller (except for the steady centrifugal forces). Equations (16b) and (17b), on the other hand, are the loads due to the blade motion when the hub is not in motion; these expressions agree with those of Ref. 7 when the pitch angle is small ($\cos\beta \approx 1$, $\sin\beta \approx \beta$ in Ref. 7) and when the blade mass distributes on the plane of $Z_B = 0$ ($\zeta = 0$, $k_{m1} = 0$ in Ref. 7). The terms containing $\dot{\theta}$ and $\ddot{\theta}$ have been retained for generality, although they are not included in Ref. 7.

IV. Aerodynamic Loads

Two-dimensional quasisteady lift L and pitching moment M are based on Eq. (18)⁵ where, referring to Fig. 5a, $U_0(t)$, $W_0(t)$, and $Q_0(t)$ denote velocities and pitching rate of a moving frame, in which blade motions are described in terms of pitching $\alpha(t)$ and plunging $h(t)$.

$$L = 2\pi\rho b U_a C [H_a + \alpha U_a + (\frac{1}{2} - a)b(\dot{\alpha} + Q_0)] + \pi\rho b^2 (d/dt) [H_a + \alpha U_a - ab(\dot{\alpha} + Q_0)] \quad (18a)$$

$$M = (a + \frac{1}{2})2\pi\rho b^2 U_a C [H_a + \alpha U_a + (\frac{1}{2} - a)b(\dot{\alpha} + Q_0)] - (\pi\rho b^3/2) U_a (\dot{\alpha} + Q_0) + \pi\rho b^3 (d/dt) [a(H_a + \alpha U_a) - b(\frac{1}{2} + a^2)(\dot{\alpha} + Q_0)] \quad (18b)$$

where

$$H_a = \dot{h} - W_0 + abQ_0 \quad U_a = -U_0 \quad C = l$$

It should be noted that Eqs. (18) hold, under quasisteady assumption, even if $U_a(t)$ is not constant⁶; that is, differentiation (d/dt) must be operated on U_a as well as H_a , Q_0 ,

and α . This is important in that this calculation accurately evaluates the noncirculatory airloads which may be significant at high frequencies in impedance computations.

When applied to the A-frame, the elastic axis is taken as the pitching axis and the relation $\alpha = \theta + \phi$ and $h = 0$ will hold. Furthermore, Q_0 is the pitching rate of the reference frame, while U_a and H_a are the Y_A and $-Z_A$ velocity components of the elastic axis relative to still air, which will be obtained in the following.

The velocity of the point P on the blade section was given by Eq. (13). The linearized form is

$$\{u_R\} = \begin{Bmatrix} \dot{u} - (e_0 + v)\Omega + V_1 - e_0\Omega_3 \\ \dot{v} + (r + u)\Omega + V_2 + r\Omega_3 \\ \dot{w} + V_3 + e_0\Omega_1 - r\Omega_2 \end{Bmatrix} + \eta \begin{Bmatrix} -\dot{v}' - \theta\dot{w}' - \Omega(1 - \theta^2/2 - \theta\phi) + \theta\Omega_2 - \Omega_3 \\ -\theta(\dot{\theta} + \dot{\phi}) - \Omega(v' + \theta w') - \theta\Omega_1 \\ \dot{\theta} + \dot{\phi} + \Omega_1 \end{Bmatrix} \quad (19)$$

Adding uniform inflow v_s in the $-Z_s$ direction, the velocity of the elastic axis relative to still air in the A-frame will be given as

$$\begin{Bmatrix} u_A \\ v_A \\ w_A \end{Bmatrix} = [\Delta_A] \left(\{u_R\}_{\eta=0} + \begin{Bmatrix} 0 \\ 0 \\ v_s \end{Bmatrix} \right) \quad (20)$$

from which U_a and H_a can be obtained as v_A and $-w_A$, respectively.

Angular velocity of the A-frame is given by

$$\begin{Bmatrix} \omega_{xA} \\ \omega_{yA} \\ \omega_{zA} \end{Bmatrix} = [\Delta_A]^T \left([\Psi]^T \begin{Bmatrix} -P \\ Q \\ \Omega - R \end{Bmatrix} + \begin{Bmatrix} 0 \\ -\dot{w}' \\ \dot{v}' \end{Bmatrix} \right) \equiv \begin{Bmatrix} \Omega_1 + \Omega w' \\ \Omega_2 - \dot{w}' \\ \Omega_3 + \Omega + \dot{v}' \end{Bmatrix} \quad (21)$$

from which Q_0 is obtained as ω_{x_A} .

Summarizing, the airloads per unit span are obtained from Eq. (18) where U_a , H_a , Q_0 , α , and h have to be replaced as follows:

$$\begin{aligned} U_a &= r(\Omega - R) + \dot{v} + U \sin \psi + V \cos \psi \\ H_a &= -v_s - \dot{w} + W + r(P \sin \psi + Q \cos \psi) \\ Q_0 &= \Omega w' - P \cos \psi + Q \sin \psi \\ \alpha &= \theta + \phi \\ h &= 0 \end{aligned} \quad (22)$$

To make the present analysis compatible with standard blade element theory, it is desired to introduce the effect of the profile and the induced drag. The inflow angle ϕ_a is defined as $\tan^{-1}(H_a/U_a)$ and the section lift L and drag D are assumed to act in the $Y_A Z_A$ plane as shown in Fig. 5b. These loads are finally resolved into the R-frame as

$$\begin{aligned} \begin{Bmatrix} F_{ax} \\ F_{ay} \\ F_{az} \end{Bmatrix} &= [\Delta_A] \begin{Bmatrix} 1 & 0 & 0 \\ 0 & \cos \phi_a & \sin \phi_a \\ 0 & -\sin \phi_a & \cos \phi_a \end{Bmatrix} \begin{Bmatrix} 0 \\ -D \\ L \end{Bmatrix} \\ &\equiv \begin{Bmatrix} -w' L \\ -D - D_i \\ L \end{Bmatrix} \end{aligned} \quad (23)$$

$$\begin{Bmatrix} M_{ax} \\ M_{ay} \\ M_{az} \end{Bmatrix} = [\Delta_A] \begin{Bmatrix} M \\ 0 \\ 0 \end{Bmatrix} \equiv \begin{Bmatrix} M \\ v' M \\ w' M \end{Bmatrix} \quad (24)$$

where

$$-D_i = L \sin \phi_a \equiv L H_a / U_a \quad D = \rho b U_a^2 C_{d0}$$

V. Blade Equations of Motion

Including the approximate gravity effects, total loads acting on the blade can be obtained as the sum of inertial, aerodynamic and gravitational loads:

$$\begin{Bmatrix} \bar{P}_x \\ \bar{P}_y \\ \bar{P}_z \end{Bmatrix} = \begin{Bmatrix} \bar{P}_x + f_x \\ \bar{P}_y + f_y \\ \bar{P}_z + f_z \end{Bmatrix} + \begin{Bmatrix} F_{ax} \\ F_{ay} \\ F_{az} \end{Bmatrix} + \begin{Bmatrix} 0 \\ 0 \\ -mg \end{Bmatrix} \quad (25)$$

$$\begin{Bmatrix} \bar{Q}_x \\ \bar{Q}_y \\ \bar{Q}_z \end{Bmatrix} = \begin{Bmatrix} \bar{Q}_x + m_x \\ \bar{Q}_y + m_y \\ \bar{Q}_z + m_z \end{Bmatrix} + \begin{Bmatrix} M_{ax} \\ M_{ay} \\ M_{az} \end{Bmatrix} + \begin{Bmatrix} -meg \\ 0 \\ 0 \end{Bmatrix} \quad (26)$$

Using these loads, blade torsional, flap bending, and chordwise bending equations of equilibrium can be written, respectively, as^{7,9}

$$-[(GJ + Tk_A^2)\phi']' + \Delta EI[(w''^2 - v''^2)\sin 2\theta/2 + v''w''\cos 2\theta] = \bar{Q}_x + \bar{Q}_y v' + \bar{Q}_z w' \quad (27a)$$

$$[(EI_I + \Delta EI \sin^2 \theta)w'' + \Delta EI(v'' \sin 2\theta/2 + \phi v'' \cos 2\theta + \phi w'' \sin 2\theta)]'' - (Tw')' = \bar{P}_z + \bar{Q}_y' \quad (27b)$$

$$[(EI_2 - \Delta EI \sin^2 \theta)v'' + \Delta EI(w'' \sin 2\theta/2 - \phi v'' \sin 2\theta + \phi w'' \cos 2\theta)]'' - (Tv')' = \bar{P}_y - \bar{Q}_z' \quad (27c)$$

where $T \equiv \Omega^2 \int_0^R m r dr$, $\Delta EI = EI_2 - EI_I$, while EI_I and EI_2 denote the flapwise bending stiffness about the Y_B axis and the chordwise bending stiffness about the Z_B axis, respectively. Substituting \bar{Q}_x , \bar{P}_z , and \bar{P}_y from Eqs. (25) and (26), the following equations are obtained:

$$\begin{aligned} &-[(GJ + Tk_A^2)\phi']' + \Delta EI[(w''^2 - v''^2)\sin 2\theta/2 \\ &+ v''w''\cos 2\theta] + mk_A^2(\ddot{\phi} + \Omega^2 \phi) + me[\ddot{w} - \theta \ddot{v} + \theta \Omega^2 v \\ &+ e_0 \Omega^2 \phi + r \Omega^2(w' - \theta v')] = m_x + M_{ax} \\ &-m[eg + k_A^2(\ddot{\theta} + \Omega^2 \theta + 2\Omega \dot{\theta} v') + e\theta(e_0 \Omega^2 - 2\Omega \dot{u})] \end{aligned} \quad (28a)$$

$$\begin{aligned} &[(EI_I + \Delta EI \sin^2 \theta)w'' + \Delta EI(v'' \sin 2\theta/2 + \phi v'' \cos 2\theta \\ &+ \phi w'' \sin 2\theta)]'' - (Tw')' + m(\ddot{w} + e\ddot{\phi}) = f_z \\ &+ F_{ax} - m(g + e\ddot{\theta} - e\Omega^2 \theta) \end{aligned} \quad (28b)$$

$$\begin{aligned} &[(EI_2 - \Delta EI \sin^2 \theta)v'' + \Delta EI(w'' \sin 2\theta/2 - \phi v'' \sin 2\theta \\ &+ \phi w'' \cos 2\theta)]'' - (Tv')' + m[\ddot{v} - e\theta \ddot{\phi} - \Omega^2(v - e\theta \phi)] \\ &= f_y + F_{ay} + m[-2\Omega \dot{u} + 2e\Omega(\dot{v}' + \theta \dot{w}') + e\theta \ddot{\theta} + \Omega^2(e_0 + 2e)] \end{aligned} \quad (28c)$$

where the Coriolis-type terms are left in the right-hand sides. When the left-hand sides of Eqs. (28) are linearized about the equilibrium position (w_0) and set equal to zero, these homogeneous equations give natural frequencies and mode shapes when the hub is fixed in the vacuum with coning. When the coupled mode shapes and the associated frequencies are denoted by $\bar{\phi}_j$, \bar{w}_j , \bar{v}_j and ω_j , respectively, blade displacements can be expressed as

$$\phi = \sum_{j=1}^{\infty} \bar{\phi}_j q_j \quad w = \sum_{j=1}^{\infty} \bar{w}_j q_j \quad v = \sum_{j=1}^{\infty} \bar{v}_j q_j \quad (29)$$

where q_j is the generalized coordinate of the j th coupled mode. According to the Rayleigh-Ritz approach, Eqs. (28) result in the following form where the orthogonality condition of the natural modes was used in the derivation:

$$m_j \ddot{q}_j + \omega_j^2 m_j q_j = Q_j \quad (j=1, 2, 3, \dots) \quad (30)$$

where

$$\begin{aligned} m_j &= \int_0^R [(k_A^2 \bar{\phi}_j + e \bar{w}_j - e \theta \bar{v}_j) \bar{\phi}_j + (\bar{w}_j + e \bar{\phi}_j) \bar{w}_j \\ &+ (\bar{v}_j - e \theta \bar{\phi}_j) \bar{v}_j] m dr \end{aligned} \quad (30a)$$

$$\begin{aligned} Q_j &= \int_0^R \{ [m_x + M_{ax} - m[eg + k_A^2(\ddot{\theta} + \Omega^2 \theta + 2\Omega \dot{\theta} v') \\ &+ e\theta(e_0 \Omega^2 - 2\Omega \dot{u})] \bar{\phi}_j + [f_z + F_{ax} - m(g + e\ddot{\theta} - e\Omega^2 \theta)] \bar{w}_j \\ &+ [f_y + F_{ay} + m[-2\Omega \dot{u} \\ &+ 2e\Omega(\dot{v}' + \theta \dot{w}') + e\theta \ddot{\theta} + \Omega^2(e_0 + 2e)] \bar{v}_j \} dr \end{aligned} \quad (30b)$$

In this paper, the radial extension of the blade has been neglected and is not included in blade equations. Although this is usually justified, the Coriolis force due to flapping may not be neglected. To account for this effect, u is approximated as

$$\begin{aligned} u &= r - \int_0^r [1 + v'^2 + w'^2]^{1/2} dr \approx -\frac{1}{2} \int_0^r [v'^2 + w'^2] dr \\ &= \sum_{j=1}^{\infty} \bar{u}_j q_j \quad \text{where} \quad \bar{u}_j \approx -\int_0^r w'_0 \bar{w}_j dr \end{aligned} \quad (31)$$

The $(v')^2$ term may be neglected if the X_R axis is relocated to the direction of mean lag angle which is constant in hover. Corresponding to this treatment, w_0 (the trim value of w) terms are retained in Eqs. (16) and (17).

VI. Rotor Impedance Calculation

The rotor hub has six degrees of freedom U, V, W, P, Q, R , each producing generally three hub forces H_s, Y_s, T_s and three hub moments M_{xs}, M_{ys}, M_{zs} as shown in Fig. 2. These loads and motions may be related in the following form when the rotor is in hover and has three or more blades:

$$\begin{Bmatrix} \Delta H_s \\ \Delta Y_s \\ \Delta T_s \\ \Delta M_{xs} \\ \Delta M_{ys} \\ \Delta M_{zs} \end{Bmatrix} = \begin{Bmatrix} \vdots \\ \vdots \\ \vdots \\ \vdots \\ \vdots \\ \vdots \end{Bmatrix} Z_R(\omega) \begin{Bmatrix} -\Delta U \\ \Delta V \\ -\Delta W \\ -\Delta P \\ \Delta Q \\ -\Delta R \end{Bmatrix} \quad (32)$$

where $\Delta U = \hat{U}e^{i\omega t}, \dots, \Delta R = \hat{R}e^{i\omega t}$. $\Delta(\)$ denotes the variations from trim, and $(\)$ generally denotes a complex amplitude. $[Z_R]$ is a kind of frequency transfer matrix, while from the standpoint of vibration analysis it may be termed as a rotor impedance matrix.¹⁰

When the blade deformations are approximated with natural modes and generalized coordinates q_j ($j=1, \dots, l$) as

$$\phi = \sum \bar{\phi}_j q_j \quad u = \sum \bar{u}_j q_j \quad v = \sum \bar{v}_j q_j \quad \bar{w} = \sum \bar{w}_j q_j$$

Eq. (30) will be written in the following matrix differential equations:

$$[A]\{\ddot{q}\} + [B]\{\dot{q}\} + [C]\{q\} = [D]\{\dot{x}\} + [E]\{x\} + \{f_0\} \quad (33)$$

where

$$\{q\} \equiv \begin{Bmatrix} q_1 \\ \vdots \\ q_l \end{Bmatrix} \quad \{x\} \equiv \begin{Bmatrix} -\Delta U \cos \psi + \Delta V \sin \psi \\ \Delta U \sin \psi + \Delta V \cos \psi \\ -\Delta W \\ -\Delta P \cos \psi + \Delta Q \sin \psi \\ \Delta P \sin \psi + \Delta Q \cos \psi \\ -\Delta R \end{Bmatrix}$$

and $[A]$ through $[E]$ denote constant matrices determined from modal parameters, blade dimensions, and rotor

operating conditions, while $\{f_0\}$ denotes the collected sums of the constant terms.

When the hub is forced to vibrate by periodic displacement $e^{i\omega t}$, $\{x\}$ will have three frequency components and, corresponding to the three forcing terms, the steady-state solution of $\{\Delta q\}$ (variation from trim) will have three frequencies, ω and $\omega \pm \Omega$, as follows:

$$\{\Delta q\} = \{\hat{q}_0'\}e^{i\omega t} + \{\hat{q}_l\}e^{i(\omega t + \psi)} + \{\hat{q}_{-l}\}e^{i(\omega t - \psi)} \quad (34)$$

On the other hand, the total hub loads can be obtained by the spanwise integration of Eqs. (25) and (26) and by the multiblade summation of them. Finally, they are transformed to the S-frame resulting in the loads variations $\Delta H_s, \Delta Y_s, \Delta T_s, \Delta M_{xs}, \Delta M_{ys},$ and ΔM_{zs} . In case of hover and $N \geq 3$, N being number of blades, it can be shown that only the frequency component of ω is transferred to the fuselage.

VII. Sample Calculations and Discussion

Numerical calculations were conducted for an articulated rectangular blade whose undeformed elastic axis lies in $X_R Z_R$ plane and coincides with both the center-of-gravity axis and aerodynamic center axis ($e_0 = e = 0, a = -1/2$). Five modes ($l=5$) were used and the natural frequencies and the associated mode shapes are shown in Table 1.

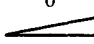
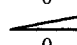


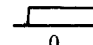
In actual blade, natural mode shapes generally couple in flapwise bending, chordwise bending, and torsion, and have nonzero values in all $\bar{\phi}_n, \bar{w}_n,$ and \bar{v}_n . Mode shapes assumed for sample calculations, however, are those of decoupled ones, as is shown in Table 1. The flapwise bending modes ($n=2,3$) and the chordwise bending modes ($n=1,4$) correspond to those of blade with flat pitch, while the fifth mode ($n=5$) is the torsional one. Control system rigidity is assumed lower than the blade torsional rigidity, as is often the case, and the control system flexibility is equivalently distributed to the blade root segment, since the feathering axis coincides with the elastic axis in this study.

Against the flat pitch assumption of the natural modes, the collective pitch angle θ of 0.150 rad was assumed in Eq. (30b). Corresponding to this θ , w'_0 (the trim value of coning angle) of 0.1055 rad is assumed, which is determined from the standard articulated-blade flapping formula. Introduction of the steady coning was intended to retain the effects of the in-plane Coriolis force ($-2m\Omega\dot{u}$) in the generalized force calculations.

In view of the foregoing, the natural mode shapes and the generalized forces are not consistent. In other words, those terms which contain θ in the left-hand side of Eq. (28) have been omitted in the modal calculations. Therefore, the results should be considered to be qualitative and the validity is limited by the assumptions used.

Results of the numerical calculations are denoted by solid lines designated as ① in Figs. 6-9. For comparison, curves noted as ②, ③, and ④, etc. are added also. Curves ② give the results where flapwise and chordwise bending modes ($n=3,4$) were simultaneously eliminated to show the effects

Table 1 Data for numerical calculations

Mode number (n)	1	2	3	4	5
Natural frequency (ω_n/Ω)	0.247	1.03	2.66	3.29	7.10
Mode shapes	$\bar{\phi}_n$ 0 \bar{w}_n 0 \bar{v}_n 	$\bar{\phi}_n$ 0 \bar{w}_n  0 \bar{v}_n 0	$\bar{\phi}_n$ 0 \bar{w}_n  0 \bar{v}_n 0	$\bar{\phi}_n$ 0 \bar{w}_n 0 \bar{v}_n 	$\bar{\phi}_n$  \bar{w}_n 0 \bar{v}_n 0
Rotor radius (R)	= 28 ft		Rotor rotational speed (Ω)		= 23.2 rad/s
Blade chord ($2b$)	= 1.366 ft		Number of blades (N)		= 4
Blade mass	= 4.5 slug		Flapping moment of inertia		= 1145 slug·ft ²
Blade mass moment	= 63 slug·ft		Feathering moment of inertia		= 0.616 slug·ft ²
Inflow ratio ($-\nu_s/R\Omega$)	= -0.049		Collective pitch angle (θ)		= 0.150 rad
Coning angle (w'_0)	= 0.1055 rad		Fuselage cg location (h)		= 8 ft

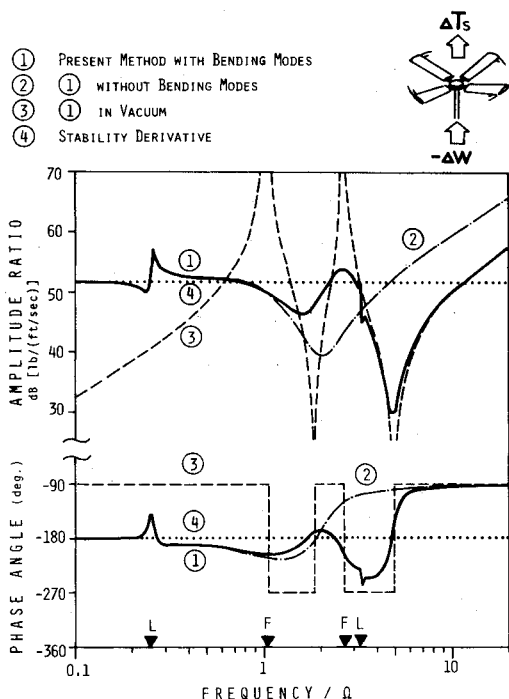


Fig. 6 Thrust variation due to shaft plunging velocity.

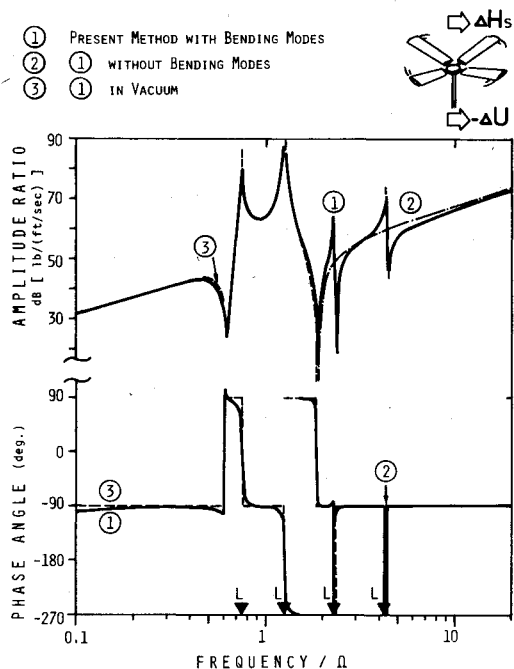


Fig. 7 In-plane force due to force-and-aft hub velocity.

of elastic deformations. Curves (3) are the results when aerodynamic loads were eliminated ($\rho=0$). Curves (4) correspond to the associated stability derivatives or the derivatives with rotor dynamics correction.¹¹ Symbol ▼ denotes the location of ω_n/Ω or $(\omega_n \pm \Omega)/\Omega$.

Figure 6 shows the thrust variations due to shaft plunging. The difference between curves (1) and (2) denotes the importance of elastic deformations. In the high-frequency range above 7Ω , curves (1) approach to curves (3), which explains the importance of the inertial loads. The coincidence of curves (1) and (4) below 0.2Ω suggest the predominance of airload due to rigid flapping.

Figure 7 gives the H -force due to in-plane displacement of the hub. Curves (1), (2), and (3) coincide closely to each other, which shows that airloads as well as elastic de-

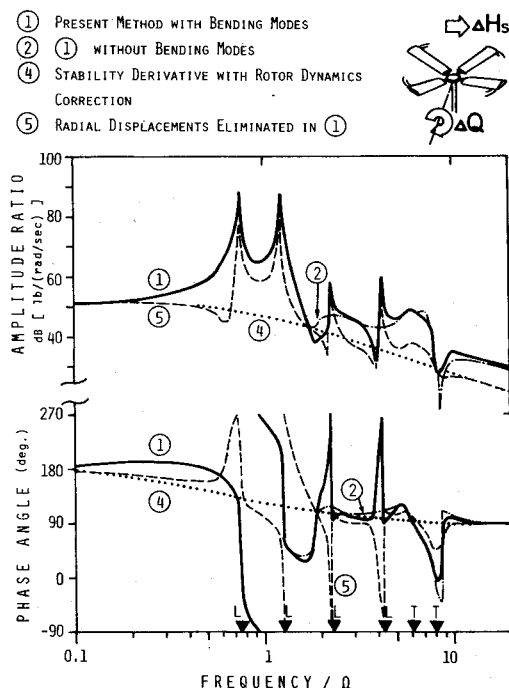


Fig. 8 In-plane force due to shaft pitching rate about hub.

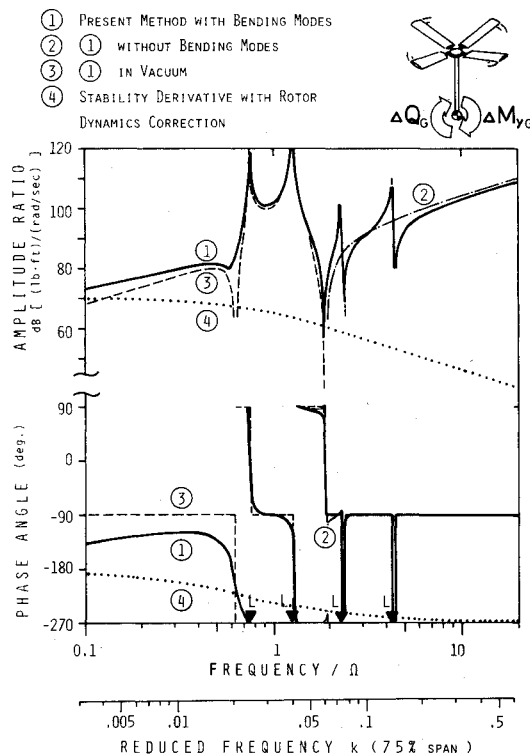


Fig. 9 Pitching moment due to shaft pitching rate about fuselage c.g.

mations are not so important except for the inertial loads due to rigid lag in all frequency ranges.

Figure 8 gives the H -force due to shaft pitching about the hub center. Coincidence of curves (1) and (2) may suggest the insignificant effect of the elastic deformations. Curves (5) in this figure are the result when the radial displacement terms ($2\Omega\dot{u}$ and $\ddot{u}-\Omega^2u$ in Eq. (16)) are intentionally eliminated from curves (1). This effect does not seem to be negligible. The slope of this curve at high frequencies shows that ΔH_s is proportional to $\Delta Q/i\omega$, which suggests that the rotor tip path stays fixed in space without regard to shaft pitching.

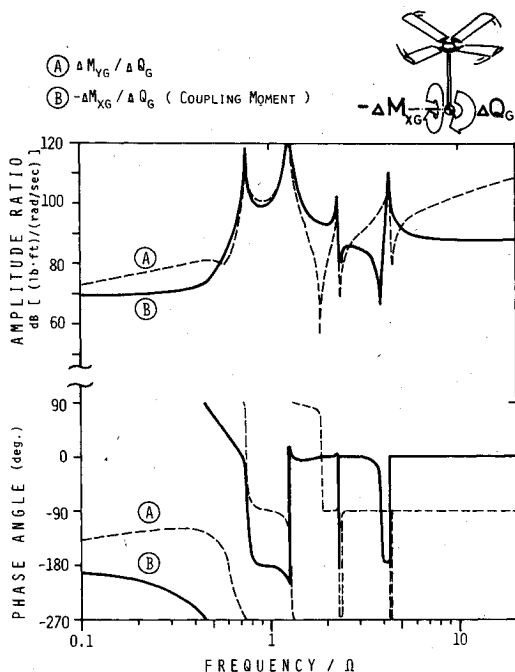


Fig. 10 Comparison of pitching and rolling moments due to pitching rate about fuselage c.g.

Figure 9 is the pitching moment due to pitching about the fuselage center of gravity (c.g.) when the hub is assumed to be located 8 ft above the c.g., and shows the combined effects of Figs. 7 and 8 for a typical helicopter. Curves ① and ② are rather close and the elastic deformations may be insignificant. Pitching moment curves ① can be considered to consist of inertial load components ③ and airload components ④. It should be understood that the stability derivative $M_{\dot{\theta}}$ (damping in pitch) describes the characteristics of this impedance only in the fairly low frequency range.

Figure 10 shows the coupling moment due to shaft pitching. Curves (A) of this figure are the same as curves ① of Fig. 9, while curves (B) shows the associated coupling (rolling) moment due to the pitching about the fuselage c.g. It can be

seen that the coupling effect may not be negligible at low frequency and also near blade natural frequencies.

In Fig. 9, the abscissa is compared with the reduced frequency k calculated at 75% span. Unsteady aerodynamic effect will increase beyond $k \approx 0.05$. However, since the inertial loads will predominate above 7Ω , those reduced frequency ranges where the unsteady aerodynamic effect is important will be restricted within rather narrow frequency ranges.

Acknowledgments

The authors are grateful to P. Friedmann of the University of California for providing valuable information on the current status of analysis in this field.

References

- ¹Friedmann, P., "Recent Developments in Rotary-Wing Aeroelasticity," *Journal of Aircraft*, Vol. 14, Nov. 1977, pp. 1027-1041.
- ²Johnston, R.A. and Cassarino, S.J., "Aeroelastic Rotor Stability Analysis," USAAMRDL-TR-75-40, Jan. 1976.
- ³McLarty, T.T., "Rotorcraft Flight Simulation with Coupled Rotor Aeroelastic Stability Analysis, Vol. 1-Engineer's Manual," USAAMRDL-TR-76-41A, May 1976.
- ⁴Anderson, W.D., Conner, F., Kretsinger, P., and Reaser, J.S., "Rexor Rotorcraft Simulation Model, Vol. 1-Engineering Documentation," USAAMRDL-TR-76-28A, July 1976.
- ⁵Bisplinghoff, R.L., Ashley, H., and Halfman, R.L., *Aeroelasticity*, Addison-Wesley, Reading, Mass., 1955, p. 272.
- ⁶Greenberg, J.M., "Airfoil in Sinusoidal Motion in a Pulsating Stream," NACA TN-1326, 1947.
- ⁷Houbolt, J.C. and Brooks, G.W., "Differential Equations of Motion for Combined Flapwise Bending, Chordwise Bending, and Torsion of Twisted Nonuniform Rotor Blades," NACA Rept. 1346, 1958.
- ⁸Hodges, D.H. and Dowell, E.H., "Nonlinear Equations of Motion for the Elastic Bending and Torsion of Twisted Nonuniform Rotor Blades," NASA TN D-7818, Dec. 1974.
- ⁹Friedmann, P., "Influence of Modeling and Blade Parameters on the Aeroelastic Stability of a Cantilevered Rotor," *AIAA Journal*, Vol. 15, Feb. 1977, pp. 149-158.
- ¹⁰Staley, J.A. and Sciarra, J.J., "Coupled Rotor/Airframe Vibration Prediction Methods," NASA SP-352, 1974, pp. 81-90.
- ¹¹Kaufman, L. and Peress, K., "A Review of Methods for Predicting Helicopter Longitudinal Response," *Journal of the Aeronautical Sciences*, Vol. 23, March 1956, p. 262.